2.6 Å resolution crystal structure of the bacterioferritin from *Azotobacter vinelandii*

He-Li Liu[a], Hui-Na Zhou[b], Wei-Man Xing[a], Jian-Feng Zhao[b], Shu-Xing Li[a], Ju-Fu Huang[b], Ru-Chang Bi[a,*]

[a]*Institute of Biophysics, Chinese Academy of Sciences, Datun Road 15, Chaoyang District, Beijing 100101, China*
[b]*Institute of Botany, Chinese Academy of Sciences, Beijing 100093, China*

Abstract **The crystal structure of the bacterioferritin from *Azotobacter vinelandii* has been determined at 2.6 Å resolution. Both the low occupancy of one iron ion in the dinuclear iron center and the deviation of its adjacent residue His130 from the center suggest migration of the iron ion from the dinuclear iron site to the inner nucleation site. The concerted movement of His130 and Glu47 may admit a dynamic gating mechanism for shift of the oxidized iron ion. Ba^{2+} binding to the fourfold channel implicates that the channel bears Fe^{2+} conductivity and selectivity to provide a route for iron access to the inner cavity during core formation.**
© 2004 Published by Elsevier B.V. on behalf of the Federation of European Biochemical Societies.

Keywords: Bacterioferritin; Dinuclear iron center; Fourfold channel; Iron entry; *Azotobacter vinelandii*

1. Introduction

Iron, an essential metal element for most biological organisms, is involved in a variety of critical processes, such as DNA synthesis, nitrogen fixation and photosynthesis [1]. As iron-storage proteins, ferritins are widespread in all domains of life, supply cells with the necessary iron, and can be also involved in cell redox-stress resistance [2], Bacterioferritins, the heme-containing ferritins isolated from bacteria, have essentially the same architecture as ferritins, assembling in a 24mer cluster to form a hollow and roughly spherical construction with a diameter of about 120 Å [2]. For both ferritins and bacterioferritins, the mechanism of iron storage, such as iron entry and exit, as well as core formation, remains unclear [2–4].

In 1973, Bulen et al. [5] isolated and crystallized a hemo-protein with non-heme iron from *Azotobacter*, Several years later, this kind of cytochrome protein was identified as a bacterioferritin and speculated as a specific iron-storage depot for nitrogenase and an electronic storage for nitrogen fixation [6]. Whereafter, the bacterioferritin from *Azotobacter vinelandii* (AvBF) has aroused research interests [7–9]. However, only the preliminary crystallographic study was performed in 1984, indicating that the crystals of AvBF belonged to the space group I432 [10].

In this paper, we report the crystal structure of the AvBF in the R3 space group. The structure has some important features different from those observed so far for other (bacterio)ferritins, such as the bacterioferritin from *Desulfovibrio desulfuricans* (DdBF) [11], and probably reveals a series of events relating to iron storage, including the shift of iron from ferroxidase center to the inner nucleation site and the selective entry of iron ions into the inner core through the fourfold channel.

2. Materials and methods

2.1. Protein preparation and crystallization

Crystals of AvBF were accidentally obtained while attempting to crystallize the Cr-containing nitrogenase component I anaerobically purified from the mutant UW3 of *Azotobacter vinelandii* [12] according to the method of Huang et al. [13]. The mutant UW_3 was grown in the modified Burk's medium containing 4.6 mM K_2HPO_4, 1.4 mM KH_2PO_4, 0.8 mM $MgSO_4 \cdot 7H_2O$, 1.7 mM NaCl, 0.6 mM $CaCl_2 \cdot 2H_2O$, 0.01 mM $Na_2CrO_4 \cdot 4H_2O$, 0.05 mM $FeSO4 \cdot 7H_2O$ (dissolved in the same concentration of citric acid) and 2% (w/v) sucrose [13].

The brick red crystals used for data collection were anaerobically grown by the microcapillary batch liquid–liquid diffusion method at 20 °C from 15 μl of 6.53 mg/ml protein solution (in 25 mM Tris buffer containing 250 mM NaCl and 1.72 mM $Na_2S_2O_4$, pH 7.4) in equilibrium with 15 μl of precipitant solution containing 5.57% PEG 8000 (w/v), 599.75 mM $MgCl_2$, 1158.9 mM NaCl, 9.23 mM $Na_2S_2O_4$, 11.57% (v/v) glycerin and 74.57 mM HEPES (pH 8.2). Matrix-assisted laser desorption ionization time-of-flight mass spectrum (MALDI-TOF MS) confirmed that the brick red crystal protein was a bacterioferritin from *Azotobacter vinelandii*. Absorption spectrum with three peaks at 416, 526 and 556 nm showed that the crystallized bacterioferritin was in a reduced state. These characterization results will be published elsewhere.

2.2. Data collection and processing

Diffraction data were collected at the Beijing Synchrotron Radiation Facility (BSRF) (Beijing, China) beamline 3W1A using a MAR345 (MAR Research, Hamburg) image plate detector with crystal-to-detector distance of 300 mm. No good cryocondition was obtained after many trials, most of which resulted in large mosaicity. As a result, all the data were collected at room temperature. The X-ray diffraction data integration and scaling were performed with the programs DENZO and SCALEPACK [14]. The data statistics is shown in Table 1. The crystals belong to the space group R3 ($a = 124.965$ Å, $b = 124.965$ Å, $c = 287.406$ Å) with eight monomers per asymmetric unit ($V_m = 2.94$ Å³/Da; 57.8% solvent). A typical '432' point group symmetry was found by calculating the self-rotation function with MOLREP [15], indicating the presence of non-crystallographic

* Corresponding author. Fax: +86-10-64871293.
E-mail address: rcbi@ibp.ac.cn (R.-C. Bi).

Table 1
Data collection and crystallographic refinement statistics

Crystal size (mm^3)	$0.28 \times 0.20 \times 0.10$
λ (Å)	0.9801
Mosaicity (°)	0.28
Independent reflections	48410
Resolution range (Å)	26.0–2.60
Completeness (%)	94.0 (95.7)[d]
$\langle I/\sigma(I)\rangle$	10.97 (2.88)[d]
R_{merge}[a]	0.105 (0.409)[d]
R_{cryst}[b]	0.196 (0.260)[d]
R_{free}[c]	0.246 (0.321)[d]
No. of protein atoms	8×1261
No. of metal atoms	32
No. of water molecules	210

[a] R_{merge}: $\Sigma|I_h - \langle I_h\rangle|/\Sigma I_h$.
[b] R_{cryst}: $\Sigma|F_o - F_c|/\Sigma F_o$, where F_o and F_c are the observed and calculated structure factor amplitudes, respectively.
[c] R_{free} values were calculated from 10% of the full reflection data set, which were not included in the refinement.
[d] Values in parentheses are for the highest resolution shell 2.69–2.60 Å.

twofold, threefold and fourfold symmetry axes, consistent with a typical 24-meric structure.

2.3. Structure determination and crystallographic refinement

The crystal structure of AvBF was solved by the molecular replacement method with the program EPMR [16]. The search template was the octamer composed of the monomers A, B, C, D, K, L, U and V from the crystal structure of *Escherichia coli* bacterioferritin (EcBF) with PDB accession code 1BFR [17]. On the first run of EPMR, the best solution was found with a crystallographic *R* factor of 0.362 and a correlation coefficient 0.675. Crystallographic refinement was carried out with CNS software package [18]. Model visualization and rebuilding were done with O [19]. The crystallographic refinement statistics on the final model is given in Table 1. The quality of the model is quite good and better than that expected at the relatively low resolution of 2.6 Å. As assessed by the program PROCHECK [20], the stereochemistry is quite satisfactory with 95.8% of the residues in most favored, 4.1% in additional, and the other 0.1% in generously allowed areas of Ramachandran plot. Coordinates have been deposited at the RCSB Protein Data Bank with accession code 1SOF.

3. Results and discussion

3.1. Overall structure of AvBF

AvBF is a spherically hollow 24mer with 432 point group symmetry (Fig. 1). As an independently biological form, the nearly spherical protomer has an external diameter of ~125 Å and an internal cavity for iron storage with a diameter of

~72 Å. Four threefold symmetry axes and three fourfold symmetry axes traverse the protomer shell, resulting in eight threefold and six fourfold channels, respectively. In addition, six twofold axes pass through the shell along the quasi-twofold axes of twelve Fe-protoporphyrin IX prosthetic groups. In the crystal structure, there are eight monomers in an asymmetric unit. Each monomer is mainly composed of a four-α-helix bundle containing a dinuclear iron site, a long loop connecting two helices of the bundle, and a short α-helix at the C terminus (Fig. 1). The C terminal residue Glu156 in each monomer was not clearly observed in the density map and was omitted from the model.

3.2. Orientation of heme group

One asymmetric unit contains four Fe-protoporphyrin IX prosthetic groups and each prosthetic group is located in the interface between two monomers related by a non-crystallographic twofold axis. In the $F_o - F_c$ electron density map with heme (in one orientation) being kept in the phasing model, no significant positive and negative peaks were observed, in particular, on the two methyl and vinyl groups, respectively. This means that the heme cofactor is located in a right position and orientation, but is not disordered or in a mixture of two orientations. Therefore, we consider that the heme preferentially binds to AvBF protein in one orientation, similar to the case of EcBF [17,21]. However, in the structures of both *Rhodobacter capsulatus* bacterioferritin (RcBF) [22] and DdBF [11], the heme groups were defined with two possible orientations each with an occupancy of about 0.50. Whether the heme group adopts two orientations or not perhaps depends on its interactions with surrounding residues. This assumption needs further investigation.

3.3. Dinuclear iron center

In the $F_o - F_c$ electron density map (Fig. 2), two peaks with different heights were detected at the hydrophilic interior of the four-helix bundle, and were assigned to iron ions Fe1 with a low occupancy and Fe2 with an occupancy of 1.00, respectively. Iterative B factor and occupancy refinements resulted into Fe1 with the averaged occupancy of 0.54 (range 0.49–0.60) and B factor 31.52 Å^2 (range 27.84–34.07 Å^2) as well as Fe2 with the averaged B factor 29.64 Å^2 (range 23.27–36.85 Å^2) in the eight subunits of an asymmetric unit where the mean Fe1–Fe2 distance is 4.13 Å (range 3.76–4.39 Å). The residues coordinated to the dinuclear iron sites include Glu127 and Glu51 as bridging ligands, Glu18 and His54 as terminal li-
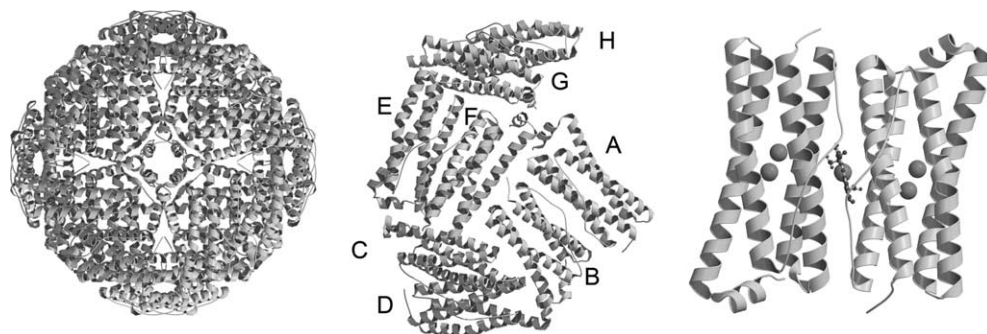

Fig. 1. Ribbon views of the AvBF 24mer along a fourfold axis (left), the eight monomers in an asymmetric unit (middle), and one dimer with a heme group located in the twofold interface and two iron ions in each monomer (right). Figs. 1, 3 and 4 in this paper were generated with Molscript [30] and Raster3D [31].
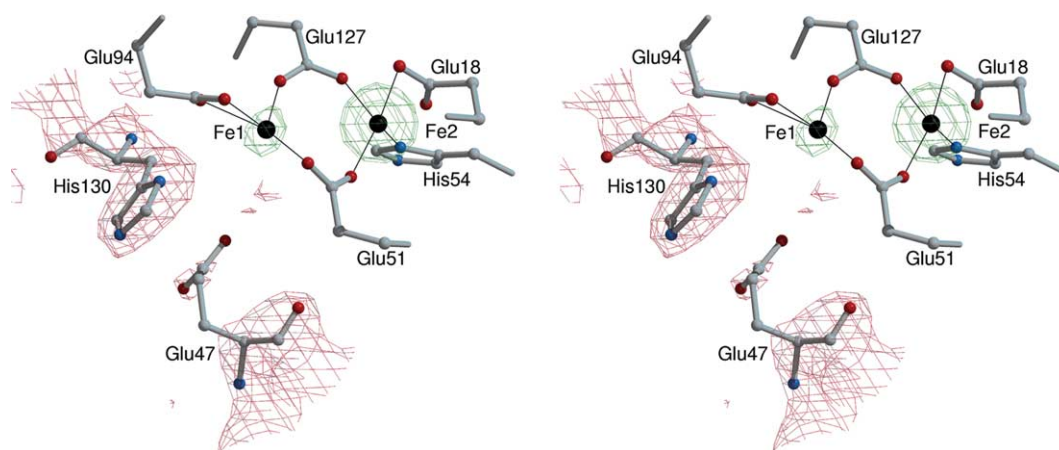
Fig. 2. Stereo view of the dinuclear iron center in the monomer G. The $F_o - F_c$ difference electron density (contoured at 7.5σ, limegreen) was calculated with the dinuclear iron omitted, and the $2F_o - F_c$ omit map (contoured at 1.2σ, sienna) calculated with His130 and Glu47 omitted for map calculation. Water molecules coordinated to Fe1 are not shown for clarity. Fig. 2 was generated with Bobscript [32] and Raster3D [31].

gands to Fe2, as well as Glu94 as a ligand to Fe1 (Fig. 2). All the residues are conserved in the ferroxidase centers of EcBF [17], DdBF [11] and RcBF [22]. Similar to the case of DdBF [11], the dinuclear iron center is located in the bottom of the so-called ferroxidase pore and can be sectioned into three layers. The top layer defines the entrance and includes Asn17, Ile20, Leu93 and Gly97; the middle layer defines the side walls and mainly includes residues Ala21, Try25 and Leu101; and the bottom layer is mainly composed of Glu47, Asp50, His54, Asp129, His130 and Ser126.

Structural comparison reveals that the dinuclear iron center of AvBF has two significant structural features different from those of EcBF [17] and DdBF [11]. First, the Fe1 atom in AvBF has both a low occupancy (0.54 on average) and a long distance to Fe2. The lower occupancy of Fe1 implicates that three steps might have continuously occurred to the dinuclear center: oxidation of Fe1 and Fe2, rupture of any μ-oxo or hydroxyl-bridge connecting them, and sequential migration of Fe1 to the inner nucleation site (possibly composed of Asp50, Glu47, and Asp129), which might have left some dinuclear sites occupied by Fe^{3+} only at the site of Fe2 as suggested by Stillman et al. [23]. From the perspective of oxidation, the Fe1–Fe2 distance of AvBF would be as short as that of the 'isolated' oxidized structure of DdBF, 3.71 Å [11]. However, the averaged Fe1–Fe2 distance is 4.13 Å and compatible with that (3.99 Å) in the reduced structure for DdBF [11]. In general, the dinuclear iron site in AvBF may represent a special partially oxidized state, to some extent, different from the 'cycled' oxidized state observed for DdBF [11], and is likely an outcome of the alternative oxidation and reduction. The low occupancy of Fe1 resulted from its oxidation during crystal installation for diffraction, while the long Fe1–Fe2 distance was from the reduction processes, including crystallization with excess of sodium dithionite as well as reduction by synchrotron radiation similar to the case of the iron derivative of the non-heme ferritin from *Escherichia coli* [23]. Furthermore, the important difference between the dinuclear iron site of AvBF and that of the 'cycled' DdBF comes from the fact that in the latter case the data were measured from flash-frozen crystals [11]. In the case of AvBF, perhaps because the oxygen exposure was shorter, the iron depletion reaction was not as

complete, and once the data collection started, the reducing effect of X-rays on the remaining iron (III) very likely stopped the reaction early on. This might also explain the longer Fe1–Fe2 distance, more typical of a reduced center, but keeping the structural changes associated with the iron depletion process. In the 'cycled' oxidized DdBF structure, any similar motion of the quasi-depleted iron (III) atoms due to X-ray induced reduction would be hindered by the fact that the crystals were frozen.

Second, the conserved residue His130 in AvBF is considered to be beyond the coordination shell of Fe1 because the distance between Fe1 and the amino nitrogen atom $N^{\delta 1}$ of His130 averages 3.45 Å (range 2.96–3.87 Å) in the eight subunits of an asymmetric unit. The large variation of His130 $N^{\delta 1}$-to-Fe1 distances may be mainly due to changes in the position of both His130 and Fe1. In contrast, its counterpart in EcBF [17] or DdBF [11] was coordinated to the metal ion in the corresponding ferroxidase center. As shown by the superposition of the residues around the dinuclear iron site from AvBF, EcBF [17] and DdBF [11] (Fig. 3), the side chain of His130 is deviating from the dinuclear metal site while the neighbor residue Glu47 swings along the reverse direction. This superposition result strongly suggests that the concerted movement of His130 and Glu47 in AvBF may constitute a gating mechanism for the
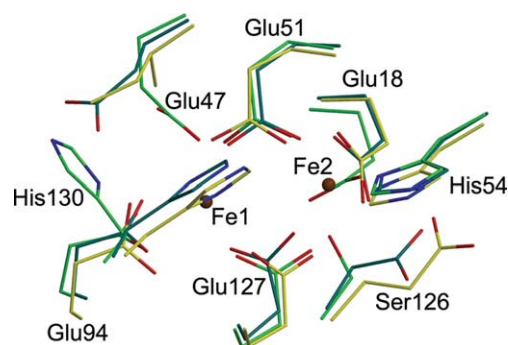

Fig. 3. Superposition of residues around the dinuclear iron site (brown spots) from AvBF (green), EcBF (blue) and DdBF (yellow). The labels refer to the AvBF residues.

shift of iron ion from the ferroxidase center to the inner nucleation site, and to a large extent supports the hypothesis that "the iron ions entered through the pore on the external surface, formed the di-iron site and from there eventually moved into the inner protein core" [2].

However, the difference in the primary sequence resulted into the concrete gating way in AvBF different from that in DdBF [11], where the movement of His59 and Glu131 was suggested to be a gating mechanism for iron migration. In the dinuclear center of AvBF, the iron atom close to His130 may migrate with the help of Glu47 after oxidation, while in DdBF the iron atom close to His59 migrates with Glu131. During the migration of iron ion, the acidic residues Glu47 (in AvBF) or Glu131 (in DdBF) near the dinuclear iron site are important for iron migration. Interestingly, four residues His130 and Glu47 (in AvBF), and His59 and Glu131 (in DdBF) are all conserved in EcBF and RcBF, which implicates that they could adopt two types of gating ways of both AvBF and DdBF. The uranyl derivative of EcBF has structurally confirmed the gating mechanism through ligand exchange between His130 and Glu47 for iron migration [24].

In addition, in the crystal structure of AvBF, the weak $2F_o - F_c$ electron density of Glu47 (Fig. 2), as well as a low occupancy of Fe1, indicates a dynamic migration of Fe1. That is likely why the crystal structure of AvBF has variable coordination environment of Fe1 in the various crystallographically independent subunits. The variable coordination environment of Fe1 concentrates on changeable Fe1-to-Glu94$O^{\varepsilon 1}$ and Fe1-to-Glu94$O^{\varepsilon 2}$ distances (range 2.35–3.18 and 1.85–2.69 Å, respectively) as well as water molecule which is coordinated to Fe1 in the subunit G but absent in the coordinate sphere of Fe1 in some subunits. In contrast, His59 remained close to the dinuclear iron site in the structure of oxidized DdBF [11] and likely reflected the final stage of the gating process with the coordinated iron mostly depleted.

3.4. Fourfold channel and its Fe^{2+} conductivity and selectivity

In the $F_o - F_c$ electron density map with all hetero atoms omitted from the phasing model, significant peaks with averaged heights of 50σ were observed on the fourfold channels and were two to three times more electron dense than those corresponding to heme iron ions. Because the AvBF sample

was purified from the mutant strain UW3 of *Azotobacter vinelandii*, Mo with different oxidation states was tentatively assigned to the strong peaks. However, residual peaks with 8σ were still detected on the positions of Mo in the $F_o - F_c$ electron density map calculated with Mo in the phasing model. Obviously, Mo is not enough to fit the assignment and heavier atoms should be adopted for these peaks. In order to determine the chemical nature of the strong peaks, an X-ray fluorescence spectrum was scanned on AvBF crystals at the BSRF, and the characteristic X-rays of Ba (Lα1, 4.466 keV; Lβ1, 4.828 keV) unambiguously indicated the presence of barium. Meanwhile, the XFS shows that the element barium is the only element heavier than Mo in AvBF crystals. The element barium may come from the reagents used for the sample preparation medium, such as sucrose (Ba content: 0.001%, Beijing Factory of Chemical Engineering) and calcium chloride dihydrate (Ba content: negligible, Beijing Yili Fine Chemistry Co. Ltd), even from glassware where $BaCO_3$ is used deliberately as additive for glassmaking. The assignment of Ba^{2+} with an occupancy of 1.00 leads to no negative or positive peaks on the Ba^{2+} positions in the $F_o - F_c$ electron density map. The reasonable averaged B factor 24.67 Å^2 of Ba^{2+} is close to that of its coordinated oxygen atoms, 22.24 Å^2.

As in the case of EcBF [17], the fourfold channel in AvBF is extremely hydrophilic with an upper layer of four Asn148 residues on the external surface of the protein shell and a lower layer of four Gln151 residues on the inner face (Fig. 4). The backbone of Asn148–Tyr149–Leu150–Gln151 located on the C terminal α-helix provides a stable scaffold to support the two layers (about 3.5 Å apart). In the structure of EcBF [17], only four Gln151 residues in the lower layer are coordinated to Mn^{2+}. In contrast, in the crystal structure of AvBF, the eight carbonyl oxygen atoms from Asn148 and Gln151 residues are all coordinated to the barium ion located on the fourfold axis (Fig. 4). The averaged distance between barium and oxygen is 3.09 Å, close to the averaged distance 3.08 Å from oxygen atom to Ba^{2+} located at the catalytic metal site in monomer B of phosphoinositide-specific phospholipase C [25].

In mammalian ferritin, the hydrophobic fourfold channel was suggested to form a "proton wire" facilitating proton transfer [26], or to provide either an exit pathway for protons during mineralization or iron leaving the protein cavity during
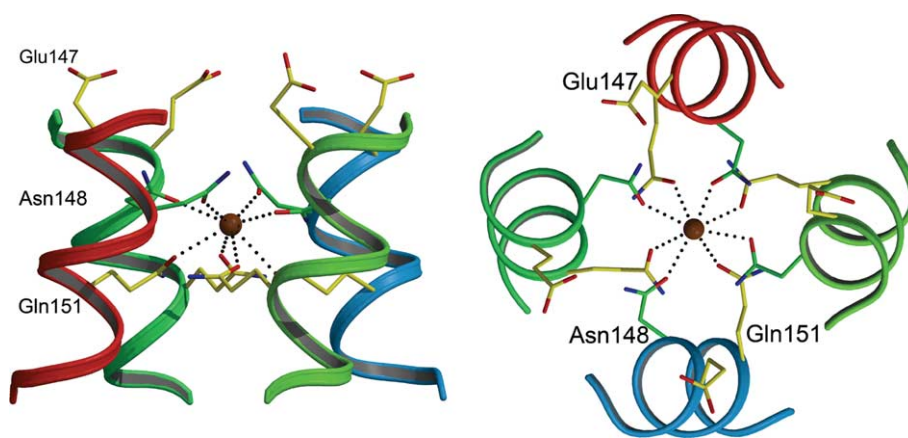

Fig. 4. Fourfold channel viewed from perspectives, respectively, perpendicular to a fourfold axis (left) and along with the axis (right). The brown spots represent the barium ion.

de-mineralization [27], even to act as the access route for dioxygen [4]. In DdBF, it is unlikely for iron to access through the fourfold channel [11], In contrast, the hydrophilic four-fold channel of AvBF could have a function for iron entry because its structural features reveal its Fe^{2+} conductivity and selectivity.

Around the entrance to this channel, four symmetry-related acidic residues Glu147 are protruding away from the AvBF surface (Fig. 4 left), thus easily uptaking ferrous ions from the surroundings and facilitating the access of these ions to the entrance of the channel. This effect is always anticipated for a cation channel and would raise the local concentration of ca-tions while lowering the concentration of anions [27]. The distance between two layers is about 3.5 Å, so that it is easy for the Fe^{2+} ion to shift from one layer to the other. Meanwhile, carbonyl oxygen atoms from either four Asn148 residues on the upper layer or four Gln151 residues on the lower layer have the capacity to accommodate a ferrous ion just as four Gln151 residues of EcBF captured Mn^{2+} [17], which has a similar size to Fe^{2+}. Therefore, two ferrous ions may simultaneously bind to each layer of residues, leading to multiple ion occupancy of the fourfold channel. Due to the short distance between the two ions, strong electrostatic repulsive forces may enhance the throughput of ferrous ions into inner cavity of AvBF. The destabilization of ions by multiple ion occupancy may be a general property of all selective ion channels [28].

The structure of the fourfold channel also reveals its selec-tivity for Fe^{2+}. When a hydrated ion enters the fourfold channel, the carbonyl oxygen atoms must substitute the water oxygen atoms to compensate for the energetic cost of dehy-dration. Like the Mn^{2+} ion accommodated by one layer of carbonyl oxygen atoms in EcBF [17], Fe^{2+} fits one layer of carbonyl oxygen atoms in the fourfold channel precisely so that the energetic costs and gains are well balanced, similar to the case of K^+ channel [28]. The stable backbone of Asn148–Tyr149–Leu150–Gln151 tightly holds two layers to prevent the carbonyl oxygen atoms from approaching close enough to accommodate a cation smaller than the Fe^{2+} ion. For a larger cation, such as Ba^{2+}, two layers of carbonyl oxygen atoms may slightly adjust their direction to the center of the fourfold channel and form a deep energy well to trap the large cation. Thus, the deep energy well formed by eight carbonyl oxygen atoms results into a blocker effect of large ions such as Ba^{2+} [29], which may inhibit the iron core formation in AvBF. However, the selectivity of the fourfold channel is limited be-cause the channel cannot exclude the permeability of ions with size close to that of Fe^{2+}. The Mn^{2+} ion in the structure of EcBF [17] is an example for this kind of limitation. Here, it is suggested that the fourfold channel bears Fe^{2+} selectivity, as the concept of K^+ selectivity was put forward although the K^+ channels allow permeation of the cations Rb^+ and Cs^+ [28].

3.5. General consideration on iron entry

In summary, the crystal structure of AvBF strongly suggests two pathways for iron entry. Both the low occupancy of Fe1 and the concerted movement of His130 and Glu47 suggest the shift of iron from the ferroxidase center to the inner nucleation site, implicating that the entry of iron may occur through the ferroxidase pore [2]. Because the hydrophobicity of the pore entrance residues Ile20 and Leu93 may limit the entry of hy-drated iron, the ferroxidase pore may only provide an entry route for a small amount of iron at initial nucleation stage. On the other hand, the observed Ba^{2+} binding to the fourfold channel implicates that the channel bears Fe^{2+} conductivity and selectivity. The potential multiple ion occupancy of the fourfold channel may lead to a high throughput for iron entry through the channel during core formation.

According to our assumption, the threefold channel, de-fined by the alternating positively and negatively charged residues Glu109, Arg117 and Glu121, is a connecting link between the preceding events at initial nucleation stage (the entry of hydrated iron through the ferroxidase pore and Fe^{3+} binding to the nucleation site) and the following events during core formation (iron entry through the fourfold channel and phosphate ion entry through the threefold channel). After completion of initial nucleation stage, Fe^{3+} may bind to the nucleation site of Glu47, Asp50 and Asp129, even to the adjacent acidic residues Asp122, Glu125, Asp132, Glu121 and Glu118 possibly due to local pH variations. The original negatively charged region (mainly composed of Glu121 and Glu118) around the bottom of the threefold channel may turn positively charged and bear more positive charges than its middle layer of the channel (composed of three symmetry related Arg117 residues). A large electrostatic potential gradient may be formed at the threefold channel, which may give rise to an electrostatic potential field directed outward from the internal cavity. At this point, phosphate ions may enter the AvBF athwart the electrostatic potential field. The access of phosphate and Fe^{2+} to the inner cavity may take place simultaneously through the threefold and fourfold channels, respectively. This may confirm the conclusion that "during iron deposition into AVBF, the phosphate and iron enter the core together to form the phosphate-Fe^{3+} mineral core" [8].

References

[1] Andrews, S.C., Robinson, A.K. and Rodriguez-Quinones, F. (2003) FEMS Microbiol. Rev. 27, 215–237.
[2] Carrondo, M.A. (2003) EMBO J. 22, 1959–1968.
[3] Theil, B.C., Takagi, H., Small, G.W., He, L., Tipton, A.R. and Danger, D. (2000) Inorg. Chim. Acta 297, 242–251.
[4] Baaghil, S., Lewin, A., Moore, G.R. and Brun, N.E.L. (2003) Biochemistry 42, 14047–14056.
[5] Bulen, W.A., Le Comte, J.R. and Lough, S. (1973) Biochem. Biophys. Res. Commun. 54, 1274–1281.
[6] Stiefel, E.L. and Watt, G.D. (1979) Nature 279, 81–83.
[7] Watt, G.D., Frankel, R.B., Papaefthymiou, G.C., Spartalian, K. and Stiefel, E.I. (1986) Biochemistry 25, 4330–4336.
[8] Watt, G.D., Frankel, R.B., Jacobs, D., Huang, H. and Papaef-thymiou, G.C. (1992) Biochemistry 31, 5672–5679.
[9] Richards, T.D., Pitts, K.R. and Watt, G.D. (1996) J. Inorg. Biochem. 61, 1–13.
[10] Zhao, B.G., Lin, Z.J., Tang, Y.Q., Li, J.D., Wang, J.W. and Tu, Y. (1984) Sci. Sin. [B] 27, 1002–1007.
[11] Macedo, S., Romao, C.V., Mitchell, E., Matias, P.M., Liu, M.Y., Xavier, A.V., LeGall, J., Teixeira, M., Lindley, P. and Carrondo, M.A. (2003) Nat. Struct. Biol. 10, 285–290.
[12] Bishop, P.E., Donna, M.L. and Hetherington, D.R. (1982) J. Bacteriol. 150, 1244–1251.

[13] Huang, J.F., Dong, Z.G., Zhang, H.F., Lv, Y.B., Zhao, Y. and Wang, Z.P. (2002) Acta Bot. Sin. 44, 297–300.

[14] Otwinowski, Z. and Minor, W. (1997) Methods Enzymol. 276, 307–326.

[15] Vagin, A. and Teplyakov, A. (1997) J. Appl. Cryst. 30, 1022–1025.

[16] Kissinger, C.R., Gehlhaar, D.K. and Fogel, D.B. (1999) Acta Crystallogr. D 55, 484–491.

[17] Dautant, A., Meyer, J.B., Yariv, J., Precigoux, G., Sweet, R.M., Kalb, A.J. and Frolow, F. (1998) Acta Crystallogr. D 54, 16–24.

[18] Brunger, A.T., Adams, P.D., Clore, G.M., De Lang, W.L., Gross, P. and Grosse-Kunstleve, R.W. (1998) Acta Crystallogr. D 54, 905–921.

[19] Jones, T.A., Zou, J.Y., Cowan, S.W. and Kjeldgaard, M. (1991) Acta Crystallogr. A 47, 110–119.

[20] Laskowski, R.A., McArthur, M.W., Moss, D.S. and Thornton, J. (1993) J. Appl. Cryst. 26, 283–291.

[21] Frolow, F., Kalb, A.J. and Yariv, J. (1994) Nat. Struct. Biol. 1, 453–460.

[22] Cobessi, D., Huang, L.S., Ban, M., Pon, N.G., Daldal, F. and Berry, E.A. (2002) Acta Crystallogr. D 58, 29–38.

[23] Stillman, T.J., Hempstead, P.D., Artymiuk, P.J., rews, S.C., Hudson, A.J., Treffry, A., Guest, J.R. and Harrison, P.M. (2001) J. Mol. Biol. 307, 587–603.

[24] Frolow, F. and Kalb, A.J. (2001) in: Handbook of Metalloproteins (Messeschmidt, A., Huber, R. and Weighard, K., Eds.) Cytochrome bl – bacterioferritin, vol. 2, pp. 782–790, John Wiley & Sons, Ltd, Chichester.

[25] Essen, L.O., Perisic, O., Lynch, D.E., Katan, M. and Williams, R.L. (1997) Biochemistry 36, 2753–2762.

[26] Takahashi, T. and Kuyucak, S. (2003) Biophys. J. 84, 2256–2263.

[27] Douglas, T. and Ripoll, D.R. (1998) Protein Sci. 7, 1083–1091.

[28] Doyle, D.A., Morais Cabral, J., Pfuetzner, R.A., Kuo, A., Gulbis, J.M., Cohen, S.L., Chait, B.T. and MacKinnon, R. (1998) Science 280, 69–77.

[29] Lesage, F. (2003) Neuropharmacology 44, 1–7.

[30] Kraulis, P.J. (1991) J. Appl. Cryst. 24, 946–950.

[31] Merritt, E.A. and Bacon, D.J. (1997) Methods Enzymol. 277, 505–524.

[32] Esnouf, R.M. (1999) Acta Crystallogr. D 55, 938–940.